Advances in Geo-Energy Research

Vol. 3, No. 4, p. 410-423, 2019

Original article

Numerical modeling of elastic wave in frequency-domain by using staggered grid fourth-order finite-difference scheme

Chao Ma[1,2], Yan Gao[1], Cheng Lu[1,2,3,4]*

[1]*Guangzhou Marine Geological Survey, China Geological Survey, Guangzhou 510098, P. R. China*

[2]*Gas Hydrate Engineering Technology Center, China Geological Survey, Guangzhou 510285, P. R. China*

[3]*Center of Oil & Natural Gas Resource Exploration, China Geological Survey, Beijing 101300, P. R. China*

[4]*School of Energy Resources, China University of Geosciences, Beijing 100083, P. R. China*

(Received November 7, 2019; revised November 27, 2019; accepted November 28, 2019; available online December 1, 2019)

Citation:
Ma, C., Gao, Y., Lu, C. Numerical modeling of elastic wave in frequency-domain by using staggered grid fourth-order finite-difference scheme. *Advances in Geo-Energy Research*, 2019, 3(4): 410-423, doi: 10.26804/ager.2019.04.08.

Corresponding author:
*E-mail: jaluch@126.com

Keywords:
Staggered grid
frequency-domain
finite-difference scheme
impedance matrix
heterogeneous medium

Abstract:
Simulation of elastic wave propagation is an important method for oil and gas exploration. Accuracy and efficiency of elastic wave simulation in complex geological environment are always the focus issue. In order to improve the accuracy and efficiency in numerical modeling, a staggered grid fourth-order finite-difference scheme of modeling elastic wave in frequency-domain is developed, which can provide stable numerical solution with fewer number of grid points per wavelength. The method is implemented on first-order velocity-stress equation and a parsimonious spatial staggered-grid with fourth-order approximation of the first-order derivative operator. Numerical tests show that the accuracy of the fourth-order staggered-grid stencil is superior to that of the mixed-grid and other conventional finite difference stencils, especially in terms of shear-wave phase velocity. Measures of mass averaging acceleration and optimization of finite difference coefficients are taken to improve the accuracy of numerical results. Meanwhile, the numerical accuracy of the finite difference scheme can be further improved by enlarging the mass averaging area at the price of expanding the bandwidth of the impedance matrix that results in the reduction of the number of grid points to 3 per shear wavelength and computer storage requirement in simulation of practical models. In our scheme, the phase velocities of compressional and shear wave are insensitive to Poisson's ratio does not occur conventional finite difference scheme in most cases, and also the elastic wave modeling can degenerate to acoustic case automatically when the medium is pure fluid or gas. Furthermore, the staggered grid scheme developed in this study is suitable for wave propagation modeling in media with coupling fluid-solid interfaces that are not resolved for previous finite difference method.

1. Introduction

In the past few decades, the reflection seismic method has developed into the main geophysical tool for oil and gas reservoir exploration, it could provide better resolution for the underground structure comparing with other geophysical methods. The essence of seismic exploration is the propagation of seismic waves in underground media, seismic wave is key to understanding characteristics of wave propagation in complex medium, and finite-difference method is one of the most effective ways of obtaining full waveform information due to its simplicity and convenience. So far, frequency-domain modeling of elastic wave has been studied for half a century. Numerical modeling of wave propagation in frequency-domain has many advantages over that in time-domain. For example, solving the visco-elastic wave equation in time-domain, is a time consuming and memory intensive work as the convolution integral should be calculated at every time interval. But in frequency-domain, as a complex to set the elastic parameters as complex, such as the velocities, the bulk density, and stiffness modulus (Arntsen et al., 1998; Štekl and Pratt, 1998; Chillara et al., 2016; Takekawa and Mikada, 2018), and the resonant phenomena can be circumvented by exerting damping factor (Min et al., 2000). Moreover, the implementation of perfectly matched layer (PML) absorbing boundary conditions (ABC) (Bérenger, 1994) provides satisfactory results both in time and frequency domain, there are additional requirement computer memory over that in time domain because of the extra need to store the splitting components in time-domain, especially for 3D cases. Besides, the application of PML in frequency-domain needs no more extra computer resources.

Another important advantage of frequency-domain mod-

https://doi.org/10.26804/ager.2019.04.08.

eling is the convenience of parallelization that has already attracted growing interests with the development of hardware and parallelization technique (Operto et al., 2007). And the most predominant superiority has been shown in manipulation of data sets acquired in multi-sources experiment where a direct solver was used (Štekl and Pratt, 1998).

Though there are many advantages of frequency-domain finite-difference technique (FDFD), it is still in its immaturity compared with that of time-domain finite-difference (TDFD) because of the intensive need of computational resources for the tremendous discrete grids in entire domain. In this regard, Jo et al. (1996) and Shin and Sohn (1998) present the optimal 9-point 2D scalar wave extrapolator operator and extended 25-point extrapolator operator, respectively. And both of them have been extended to elastic wave modeling (Štekl and Pratt, 1998; Min et al., 2000; Wang and Liang, 2018). The number of grid points per wavelength required by Štekl and Pratt (1998) is larger than four, and their optimal coefficients of the finite difference (FD) scheme varies with Poisson's ratio, and yet the compressional and shear wave phase velocities couldn't converge to their true values simultaneously by mixed-grid operator. The 25-point weighted-averaging FD operator has made a great progress in the simultaneous convergence of compressional and shear wave phase velocities, and the number of grid can be lowered to 3.3 points per wave length for a wide range of Poisson's ratio. But the 25-point FD scheme is not quite efficient in complex medium modeling because of the differential form of second-order partial derivative terms, which may also lead to amplitude distortion at source location. Moreover, all of the FD schemes described above appear to be inefficient when dealing with strong contrast medium and pure fluid bearing problems. Therefore, for pure fluid bearing problems that are usually the case in practical application, one has to solve acoustic wave equation and the solid-fluid interfaces the treated with special measures which result in complicated impedance matrix with full rank (Matuszyk et al., 2012).

Actually, some problems listed above can be solved by staggered-grid FD scheme. It is well known that the staggered grid TDFD method is conductive to elastic wave simulation in heterogeneous formation with arbitrary Poisson's ratio (Madariaga, 1976; Virieux, 1984, 1986). In the study, we introduce an elastic wave modeling method using staggered-grid FDFD stencils. As usual as conventional difference scheme (Pratt, 1990a, 1990b), the staggered-grid TDFD method was first fulfilled in second-order approximation (Virieux, 1984), and was later modified to fourth-order (Dablain, 1986; Levander, 1988). Until now, nearly most work are on the basis of conventional grid in frequency-domain. Hustedt et al. (2004) compared the efficiency and accuracy between the mixed-grid scheme and the fourth-order staggered grid scheme in case of acoustic simulation.

For now, staggered grid FDFD method is not widely used in modeling of elastic wave compared with TDFD, most likely due to the low accuracy of second order approximation. Gelis et al. (2007) adopted a second-order rotated staggered grid scheme (Saenger et al., 2000) in full waveform inversion. In this study, we first introduce the basic procedure of constructing the parsimonious form of first-order velocity-stress equation with second-order. Secondly, we extended the FD stencil to fourth-order, and employ the lumped mass acceleration averaging method to alleviate the grid dispersion at the same time. Next, the staggered grid scheme proposed in this study is applied to modeling medium of pure fluid, and medium including coupled interfaces of solid and fluid. Finally, a complex model developed by previous authors is used to check the validity and accuracy of our FDFD scheme.

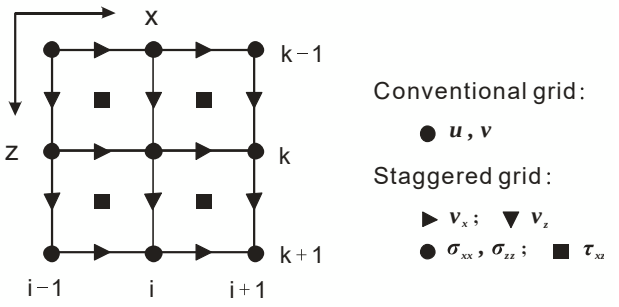

Fig. 1. Elementary grid cells for the conventional grid scheme and staggered grid scheme in 2D.

2. The staggered grid stencil for elastic wave equation

In a 2D Cartesian coordinate system (x,z), where x-axis is positive to the right horizontally and z-axis is positive downward vertically (Fig. 1), the first-order elastic wave equation (Virieux, 1986) including body force can be written as follows:

$$\begin{aligned} i\omega\rho v_x + \frac{\partial \sigma_{xx}}{\partial x} + \frac{\partial \tau_{zx}}{\partial z} + f_x = 0 \\ i\omega\rho v_z + \frac{\partial \tau_{xz}}{\partial x} + \frac{\partial \sigma_{zz}}{\partial z} + f_z = 0 \end{aligned} \tag{1a}$$

$$\begin{aligned} i\omega\sigma_{xx} + c_{11}\frac{\partial v_x}{\partial x} + c_{13}\frac{\partial v_z}{\partial z} = 0 \\ i\omega\sigma_{zz} + c_{13}\frac{\partial v_x}{\partial x} + c_{33}\frac{\partial v_z}{\partial z} = 0 \\ i\omega\tau_{xz} + c_{55}\frac{\partial v_x}{\partial z} + c_{55}\frac{\partial v_z}{\partial x} = 0 \end{aligned} \tag{1b}$$

where, $v_x(x,z,\omega)$ and $v_z(x,z,\omega)$ are temporal Fourier components of horizontal and vertical velocity vector, respectively; $\sigma_{xx}(x,z,\omega)$, $\sigma_{zz}(x,z,\omega)$ and $\tau_{xz}(x,z,\omega)$ are stress components; ω is circular frequency; ρ is the bulk density; and c_{11}, c_{13}, c_{33} and c_{55} are elastic stiffness modulus; f_x and f_z are body forces.

The equations of system (1) could be discretized on the staggered grid by defining the particle velocity and stress as well as the bulk density and stiffness modulus in the different position of the grid. We followed the grid stencil of Virieux (1986) shown in Fig. 1, while the displacements on a conventional grid is in position of the vertex.

Applied the PML (Ma et al., 2014) to equations of system (1), they can be modified as follows:

$$\begin{aligned}
&\rho(i+1/2\,,k)\,[i\omega+d_x(i+1/2\,)]\,v_{xx}(i+1/2\,,k,\omega)\\
&+\frac{\partial\sigma_{xx}}{\partial x}(i+1/2\,,k,\omega)+f_x=0\\
&\rho(i+1/2\,,k)\,[i\omega+d_z(k)]\,v_{xz}(i+1/2\,,k,\omega)\\
&+\frac{\partial\tau_{xz}}{\partial z}(i+1/2\,,k,\omega)+f_x=0\\
&\rho(i,k+1/2\,)\,[i\omega+d_x(i)]\,v_{zx}(i,k+1/2\,,\omega)\\
&+\frac{\partial\tau_{xz}}{\partial x}(i,k+1/2\,,\omega)+f_z=0\\
&\rho(i,k+1/2\,)\,[i\omega+d_z(k+1/2\,)]\,v_{zz}(i,k+1/2\,,\omega)\\
&+\frac{\partial\sigma_{zz}}{\partial z}(i,k+1/2\,,\omega)+f_z=0
\end{aligned}\tag{2}$$

where d_x and d_z are damp function for PML, $v_{xx}(i+1/2\,,k,\omega)$ and $v_{xz}(i+1/2\,,k,\omega)$ and are auxiliary variables of horizontal velocity components with $v_x(i+1/2\,,k,\omega)=v_{xx}(i+1/2\,,k,\omega)+v_{xz}(i+1/2\,,k,\omega)$.

3. The discretization of first-order elastic wave equation on staggered grid

3.1 Second-order approximation of derivatives and the discrete wave equation

In Fourier-domain, we discretize the Eq. (2) using approximation of second-order central difference by partial derivatives:

$$\begin{aligned}
&\frac{\partial\sigma_{xx}}{\partial x}(i+1/2\,,k,\omega)\approx\frac{1}{\Delta x}\,[\sigma_{xx}(i,k,\omega)+\sigma_{xx}(i+1,k,\omega)]\\
&\frac{\partial\tau_{xz}}{\partial z}(i+1/2\,,k,\omega)\approx\frac{1}{\Delta z}\\
&[\tau_{xz}(i+1/2\,,k+1/2\,,\omega)+\tau_{xz}(i+1/2\,,k-1/2\,,\omega)]\\
&\frac{\partial\tau_{xz}}{\partial x}(i,k+1/2\,,\omega)\approx\frac{1}{\Delta x}\\
&[\tau_{xz}(i+1/2\,,k+1/2\,,\omega)+\tau_{xz}(i-1/2\,,k+1/2\,,\omega)]\\
&\frac{\partial\sigma_{zz}}{\partial z}(i,k+1/2\,,\omega)\approx\frac{1}{\Delta z}\,[\sigma_{zz}(i,k,\omega)+\sigma_{zz}(i,k+1,\omega)]
\end{aligned}\tag{3}$$

where Δx and Δz are spatial sampling intervals. Substituting the equations of system (3) to Eq. (2) and with $S_x=i\omega+d_x$ and $S_z=i\omega+d_z$, equation system (2) can be rewritten as:

$$\begin{aligned}
&v_{xx}(i+1/2\,,k,\omega)+f_x=-\frac{\sigma_{xx}(i,k,\omega)+\sigma_{xx}(i+1,k,\omega)}{S_x(i+1/2\,)\rho(i+1/2\,,k)\Delta x}\\
&v_{xz}(i+1/2\,,k,\omega)+f_x=\\
&-\frac{\tau_{xz}(i+1/2\,,k+1/2\,,\omega)+\tau_{xz}(i+1/2\,,k-1/2\,,\omega)}{S_z(k)\rho(i+1/2\,,k)\Delta z}\\
&v_{zx}(i,k+1/2\,,\omega)+f_z=\\
&-\frac{\tau_{xz}(i+1/2\,,k+1/2\,,\omega)+\tau_{xz}(i-1/2\,,k+1/2\,,\omega)}{S_x(i)\rho(i,k+1/2\,)\Delta x}\\
&v_{zz}(i,k+1/2\,,\omega)+f_z=-\frac{\sigma_{zz}(i,k,\omega)+\sigma_{zz}(i,k+1,\omega)}{S_z(k+1/2\,)\rho(i,k+1/2\,)\Delta z}
\end{aligned}\tag{4}$$

After pair wise summation of Eq. (4), the left hand side term will be $v_x(i+1/2\,,k,\omega)+f_x$ and $v_z(i,k+1/2\,,\omega)+f_z$, the discretized equations of system (1b) are as follows:

$$\begin{aligned}
&\sigma_{xxx}(i,k,\omega)=-\frac{c_{11}(i,k)}{S_x(i)\Delta x}\,[v_x(i+1/2\,,k,\omega)+v_x(i-1/2\,,k,\omega)]\\
&\sigma_{xxz}(i,k,\omega)=-\frac{c_{13}(i,k)}{S_z(k)\Delta z}\,[v_z(i,k+1/2\,,\omega)+v_z(i,k-1/2\,,\omega)]\\
&\sigma_{zzx}(i,k,\omega)=-\frac{c_{13}(i,k)}{S_x(i)\Delta x}\,[v_x(i+1/2\,,k,\omega)+v_x(i-1/2\,,k,\omega)]\\
&\sigma_{zzz}(i,k,\omega)=-\frac{c_{33}(i,k)}{S_z(k)\Delta z}\,[v_z(i,k+1/2\,,\omega)+v_z(i,k-1/2\,,\omega)]\\
&\sigma_{xzx}(i+1/2\,,k+1/2\,,\omega)=-\frac{c_{55}(i+1/2\,,k+1/2\,)}{S_x(i+1/2\,)\Delta x}\\
&[v_z(i+1,k+1/2\,,\omega)+v_z(i,k+1/2\,,\omega)]\\
&\sigma_{xzz}(i+1/2\,,k+1/2\,,\omega)=-\frac{c_{55}(i+1/2\,,k+1/2\,)}{S_z(k+1/2\,)\Delta z}\\
&[v_x(i+1/2\,,k+1,\omega)+v_x(i+1/2\,,k,\omega)]
\end{aligned}\tag{5}$$

As before, we sum the Eq. (5), and sort out three equations, the left hand side are $\sigma_{xx}(i,k,\omega)$, $\sigma_{zz}(i,k,\omega)$ and $\sigma_{xz}(i+1/2\,,k+1/2\,,\omega)$, respectively. Now we substitute the consolidated Eq. (5) to Eq. (4), then we have the parsimonious form as follows:

$$\begin{aligned}
v_x(i+1/2\,,k,\omega)=&-A_3v_x(i-1/2\,,k,\omega)\\
&-A_8v_x(i+1/2\,,k-1,\omega)\\
&+(A_1+A_3+A_6+A_8)\\
&\times v_x(i+1/2\,,k,\omega)\\
&-A_6v_x(i+1/2\,,k+1,\omega)\\
&-A_1v_x(i+3/2\,,k,\omega)\\
&-(A_4+A_7)v_z(i,k-1/2\,,\omega)\\
&+(A_4+A_5)v_z(i,k+1/2\,,\omega)\\
&+(A_2+A_7)v_z(i+1,k-1/2\,,\omega)\\
&-(A_2+A_5)v_z(i+1,k+1/2\,,\omega)\\
v_z(i,k+1/2\,,\omega)=&-B_3v_z(i-1,k+1/2\,,\omega)\\
&-B_8v_z(i,k-1/2\,,\omega)\\
&+(B_1+B_3+B_6+B_8)v_z(i+1/2\,,k,\omega)\\
&-B_6v_z(i,k+3/2\,,\omega)\\
&-B_1v_z(i+1,k+1/2\,,\omega)\\
&-(B_4+B_7)v_x(i-1/2\,,k,\omega)\\
&+(B_4+B_5)v_x(i-1/2\,,k+1,\omega)
\end{aligned}\tag{6a}$$

$$+(B_2+B_7)v_x(i+1/2\,,k,\omega)$$
$$-(B_2+B_5)v_x(i+1/2\,,k+1,\omega) \tag{6b}$$

The parsimonious form for fourth-order FD scheme could be derived in the same way, and the expressions of coefficients A_i and B_i for both second-order and fourth-order FD schemes are listed in Appendix.

The fourth-order staggered grid FD scheme is a FD scheme no more than 29 points, and the non-zero elements in each row are no more than 33. At last, elastic wave equations can be written in terms of the following form:

$$S(\omega)\cdot v(\omega)=f \tag{7}$$

where, $S(\omega)$ is the large sparse matrix at different frequency ω; $v(\omega)$ is the unknown wavefield; and f is the source term. Both direct solvers and iterate solvers (Erlangga, 2006; Plessix, 2007; Plessix, 2009) can be used to solve the equations of linear system (7).

3.2 Determination of the averaging and optimal FD coefficients

To minimize the effect of grid dispersion, we must derive the dispersion relationship first. Considering a vector plane-wave solution in a homogeneously infinite medium with velocity of $v^{\omega}=V^{\omega}e^{ik\cdot r}$, where $V=(V_x^{\omega},V_z^{\omega})$ are vector of horizontal and vertical velocity components, respectively; $k=(k_x,k_z)$ is the wavenumber vector and $r=(x,z)$ represents the position vector. And the staggered grid FD scheme for homogeneous elastic wave equations reduces to a matrix form

$$\begin{bmatrix}\omega^2M-(\alpha^2F_{XX}+\beta^2F_{XZ}) & (\alpha^2-\beta^2)F_Z\\ (\alpha^2-\beta^2)F_X & \omega^2M-(\alpha^2F_{ZX}+\beta^2F_{ZZ})\end{bmatrix}\begin{bmatrix}V_x^{\omega}\\V_z^{\omega}\end{bmatrix}=0 \tag{8}$$

where M is the mass acceleration operator; V_x^{ω} and V_z^{ω} are compressional and shear wave velocities; F_{XX}, F_{XZ} , F_{ZX}, F_{ZZ} and F_X, F_Z are FD operators of spatial derivative. In the case of homogeneous isotropic medium, $F_X=F_Z$, $F_{XZ}=F_{ZX}$, $F_{XX}=F_{ZZ}$ and have forms of

$$\begin{aligned}F_{XX}=&2\{a_1^2+a_2^2-a_1^2\cos(k_x)-a_2^2\cos(3k_x)\\&+2a_1a_2[\cos(k_x)-\cos(2k_x)]\}\end{aligned} \tag{9}$$

$$\begin{aligned}F_{XZ}=&2\{a_1^2+a_2^2-a_1^2\cos(k_z)-a_2^2\cos(3k_z)\\&+2a_1a_2[\cos(k_z)-\cos(2k_z)]\}\end{aligned} \tag{10}$$

$$\begin{aligned}F_X=&4\{a_1^2\sin(k_x/2)\ \sin(k_z/2)\\&+a_2^2\sin(3k_x/2)\ \sin(3k_z/2)\\&+a_1a_2[\sin(k_x/2)\ \sin(3k_z/2)\\&+\sin(3k_x/2)\ \sin(k_z/2)\ ]\}\end{aligned} \tag{11}$$

In Eq. (8), the term of M can be obtained through two kinds of averaging scheme, which are mass weighted-averaging without additional costs (13-point FD scheme) and that of mass weighted-averaging with additional costs (29-point FD scheme). The former can be written as:

$$\begin{aligned}M=&c_1+c_2[\cos(k_x)+\cos(k_z)]\\&+c_3[\cos(2k_x)+\cos(2k_z)]\\&+c_4[\cos(3k_x)+\cos(3k_z)]\end{aligned} \tag{12}$$

and the later can be described as:

$$\begin{aligned}M=&c_1+c_2[\cos(k_x)+\cos(k_z)]\\&+c_3[\cos(2k_x)+\cos(2k_z)]\\&+c_4[\cos(3k_x)+\cos(3k_z)]\\&+c_5[\cos(k_x+k_z)+\cos(k_x-k_z)]\\&+c_6[\cos(2k_x+2k_z)+\cos(2k_x-2k_z)]\\&+c_7[\cos(2k_x+k_z)+\cos(2k_x-k_z)\\&+\cos(k_x+2k_z)+\cos(k_x-2k_z)]\end{aligned} \tag{13}$$

where, $k_x=k\Delta\cos(\theta)=2\pi K\cos(\theta)$, $k_z=k\Delta\sin(\theta)=2\pi K\sin(\theta)$. If the grid is square, under the condition of the determinant equals to zero, the phase velocity is expressed as $v_{\mathrm{ph}}=\omega/k$.

$$\begin{aligned}\frac{v_{p\mathrm{ph}}}{v_p}&=\frac{1}{2\pi K}\sqrt{\frac{B+\sqrt{B^2-4AC}}{2A}}\\ \frac{v_{s\mathrm{ph}}}{v_s}&=\frac{1}{2\pi KR}\sqrt{\frac{B-\sqrt{B^2-4AC}}{2A}}\end{aligned} \tag{14}$$

where, $A=M^2$, $B=M(1+R^2)(F_{XX}+F_{XZ})$, $C=(F_{XX}+R^2F_{XZ})(R^2F_{XX}+F_{XZ})-M^2(1-R^2)^2$, σ is the Poisson's ratio, $R=v_s/v_p=\sqrt{(0.5-\sigma)/(1-\sigma)}$. While the group velocity could be obtained by $v_{\mathrm{gr}}=\partial\omega/\partial k$ (Štekl and Pratt, 1998).

In this study, the Gauss-Newton method (Lines and Treitel, 1984; Min et al., 2000) is used to determine the mass weighting coefficients and optimal FD coefficients. It should be pointed out that in two mass weighting schemes, usually the first one is favorable due to easy realization. For large scale problems, the second one may be selected for higher accuracy needed. In our case, the initial guess of the optimal coefficients is as follows: c_1=1, c_2=0, c_3=0, c_4=0, c_5=0, c_6=0, c_7=0, a_1=9/8, a_2=-1/24.

The two sets of optimal coefficients with different mass averaging schemes after the optimization by using Gauss-Newton method is listed in Table 1.

3.3 Dispersion analysis

With all the weighting coefficients prepared, firstly, it is about to check the dispersion relations by comparing the phase and group velocities as a function of the grid numbers per shear wavelength.

Fig. 2 shows the result of dispersion curves by using 25-point weighted-averaging FD stencil (Min et al., 2000) for a Poisson's ratio of 0.48, which represents for an extreme situation. It is shown that as the increasing of the Poisson's ratio, the velocity of shear wave tends to be dispersive. This also demonstrates that the scheme of 25-point weighted-averaging FD stencil is not independent of Poisson's ratio. For

Table 1. Two sets of optimal coefficients with different mass averaging schemes.

c_1	c_2	c_3	c_4	c_5	c_6	c_7	a_1	a_2
0.770568	0.180138	-0.108776	0.030163	0	0	0	1.092386	-0.053935
0.784123	0.100338	-0.057946	0.006473	0.064332	0.00126	-0.01288	1.058806	-0.039234

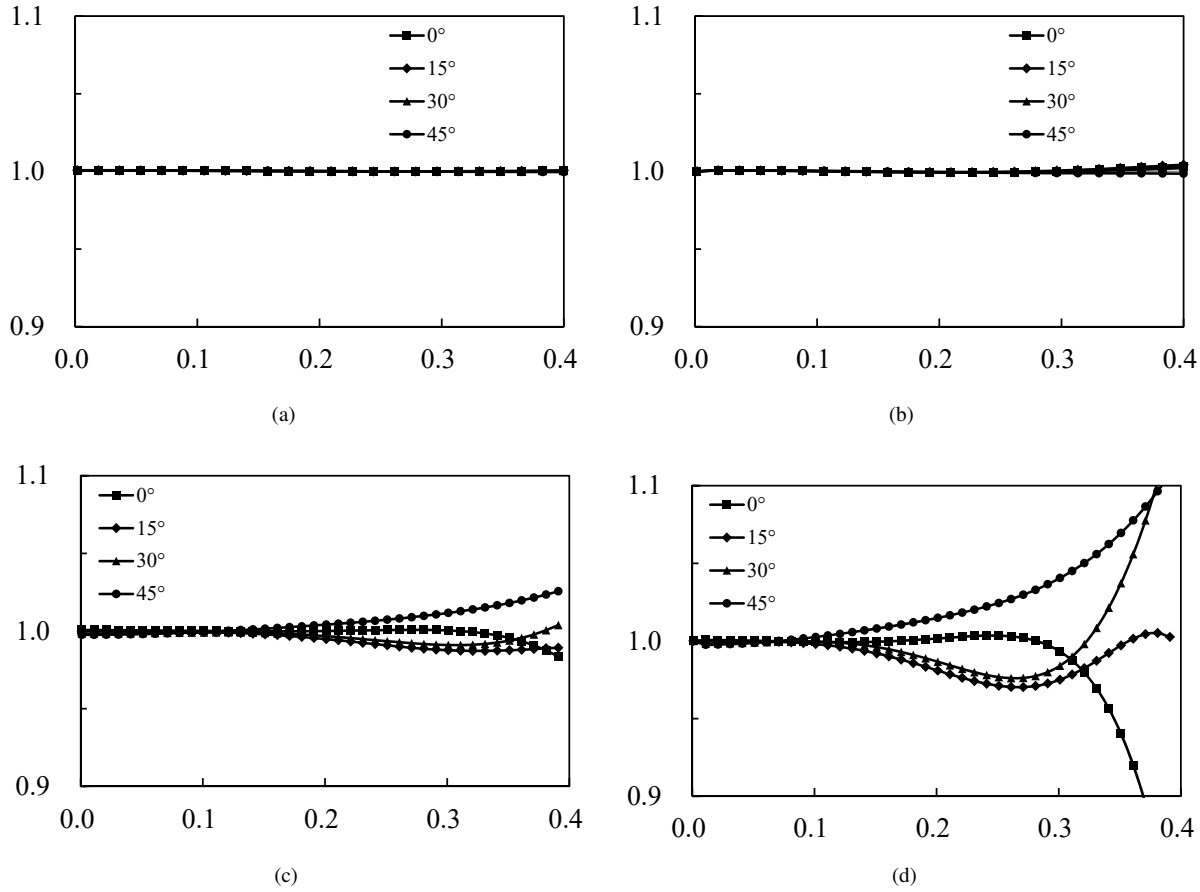

Fig. 2. Dispersion curves of phase velocity and group velocity by using 25-point FD scheme (Min et al., 2000) when the Poisson's ratio is 0.48.

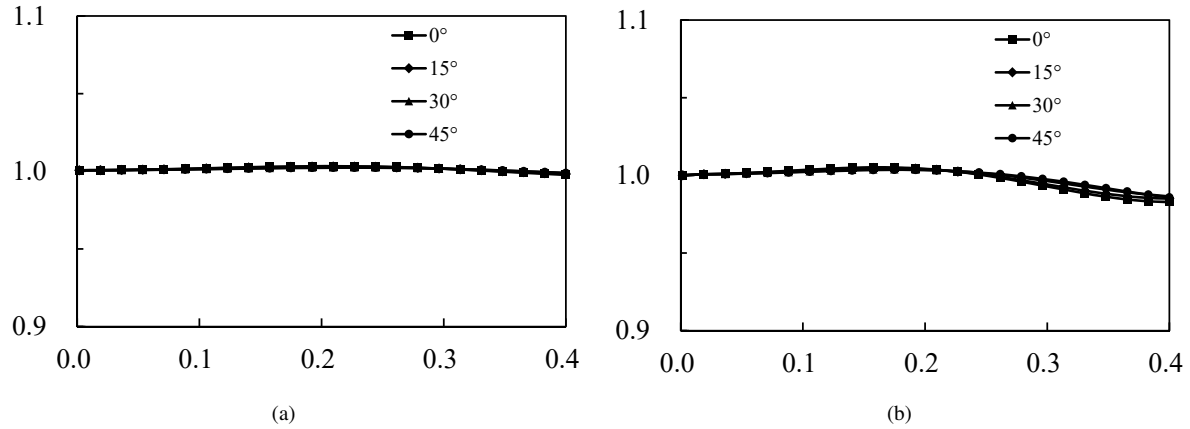

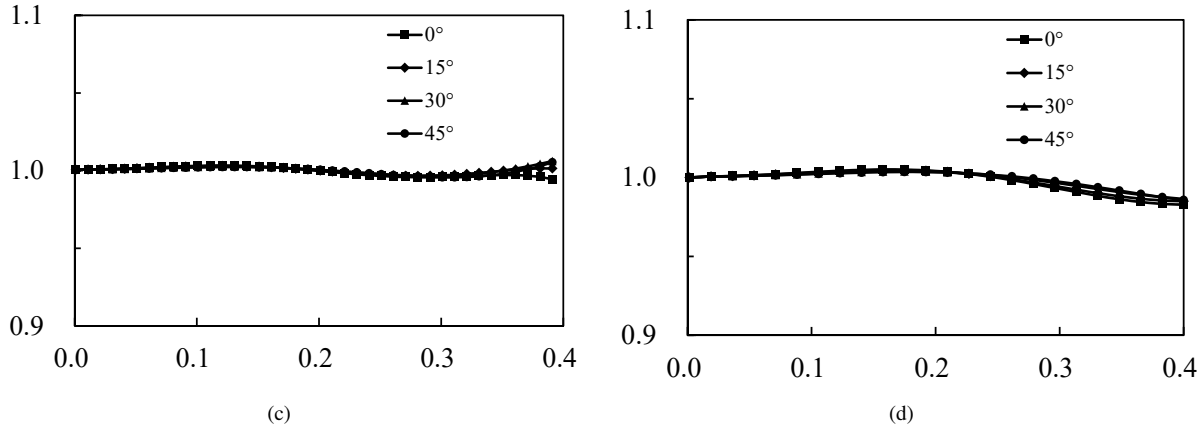

Fig. 3. Dispersion curves of phase velocity and group velocity by using the staggered grid fourth-order FD stencil with 13-point mass weighted-averaging while the dispersion relationship of S-wave is independent of Poisson's ratio.

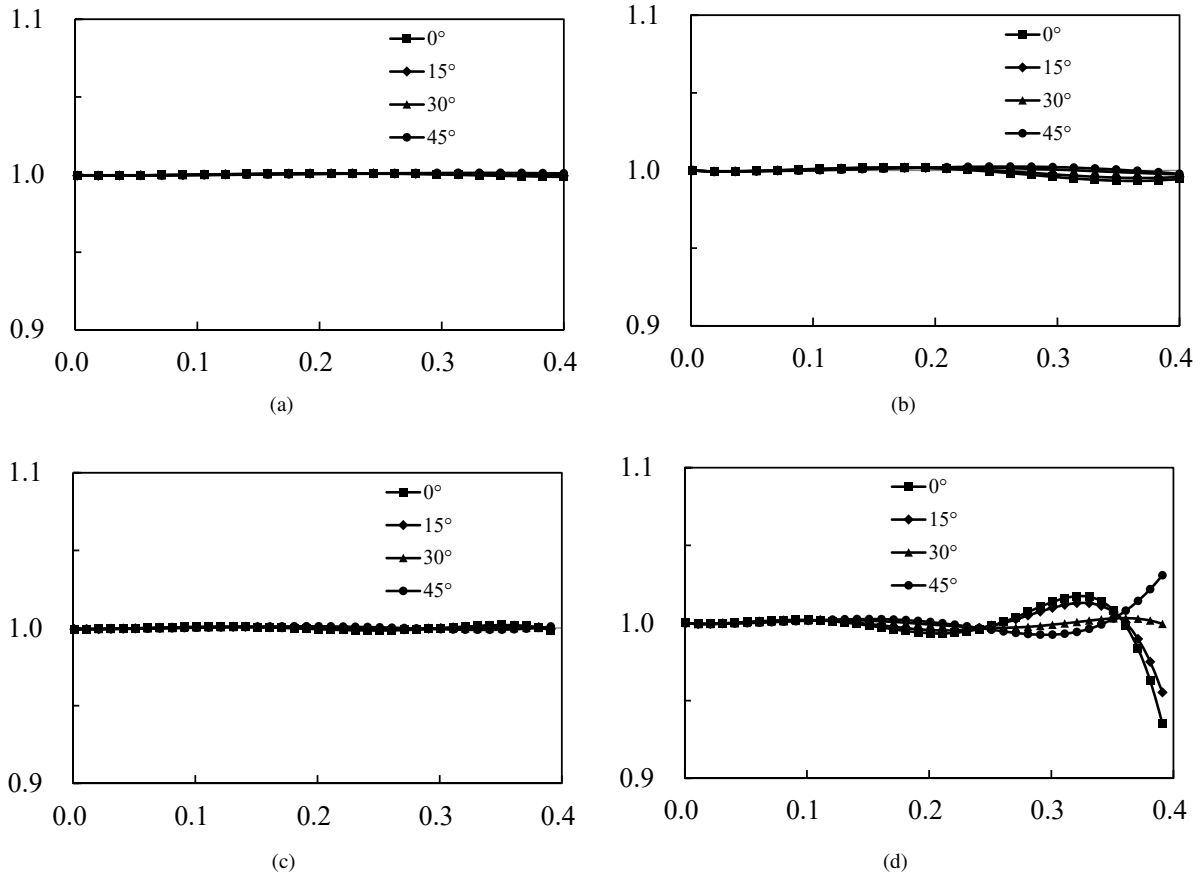

Fig. 4. Dispersion curves of phase velocity and group velocity by using the staggered grid fourth-order FD stencil with 29-point mass weighted-averaging while the dispersion relationship of S-wave is independent of Poisson's ratio.

Table 2. Model parameters of the vertical-step model.

Layer	Density	V_P	V_S
1	2.0 g/cm^3	1800 m/s	1000 m/s
2	2.4 g/cm^3	3000 m/s	1600 m/s
3	2.7 g/cm^3	4000 m/s	2200 m/s

this problem, we bring to the staggered grid optimal fourth-order FD stencil with 13-point weighted-averaging, and the results are exhibited in Fig. 3. It's clear that the accuracy and dispersion are improved obviously, and the dispersion curves with 29-point weighted-averaging are presented in Fig. 4. It is clearly that the 29-point weighted-averaging scheme behaves better for a higher accuracy, but it will enlarge the numerical bandwidth of the impedance matrix and hence increases the computational cost and memory requirement.

4. Numerical examples

4.1 The vertical-step model

We compare the fourth-order staggered grid FDFD scheme with TDFD scheme for a vertical-step model (Min et al., 2000; Hustedt et al., 2004). The vertical-step model contains three homogeneous media with a horizontal layer and a vertical step layer. The model parameters are shown in Table 2. The size of the model is 1500 m × 1500 m and discretized with a uniform mesh spacing of 7.5 m, where five layers of PML ABCs are applied at four edges. Noting the lowest shear wave velocity and considering the model size, we set the total time of seismogram to 2.5 s, and the maximum frequency could be as high as 54 Hz, then the lowest grid points per shear wavelength is only 2.47. We put a concentrated force source at the position of x = 750 m and z = 75 m, the receivers are laid up parallelly as shown in Fig. 5b. Then we run the forward procedure for 135 frequencies in the 0∼54 Hz frequency range. Wavefield of horizontal component and vertical component at 16 Hz are shown in Fig. 5 and the synthetic seismograms between FDFD and TDFD schemes are displayed in Figs. 6∼7.

From Figs. 6∼7, the same seismogram patterns are displayed from both left and right panel. The direct *P*-wave and *S*-wave appear at the same time but with a little difference at the source location. And the *PP*, *PS*, *SP* and *SS*-reflections show the same arrival time either. The stepped conformation can be reflected by the white circles in Fig. 6, the amplitude from the result of FDFD is weaker compared with the result from TDFD, which may on account of the rarity of frequency sampling and the lack of PML layers (see the white dashed line in Fig. 7b). From the above seismograms, even the shear wave dispersion is rarely seen with only 2.47 grid points per shear wavelength. In a word, the fourth-order staggered grid FD scheme shows strong stability when modeling in complex isotropic medium.

4.2 Modeling in Marmousi model

A comparison of accuracy between acoustic staggered grid second-order and fourth-order schemes for the Marmousi model has been conducted by Pan et al. (2012). The result turned out the fourth-order scheme holds a satisfactory stability and consistency for strong inhomogeneous medium. We complete the elastic modeling for Marmous model and make a comparison between the results from second-order scheme and fourth-order. The size of Marmous model is reshaped in the numerical operation, as the P-wave velocity is shown in Fig. 8a, Taking the medium as Poisson's body for simplicity, so $v_s = v_p/1.732$. And the density is given by Gardner's method, i.e., $\rho = 310 v_p^{0.25}$.

In both cases, we perform the simulation among two sets of grids, that is $\Delta x = \Delta z = 25$ m for the spatial grid stencil of 321 × 201, and $\Delta x = \Delta z = 12.5$ m for 641 × 401, the

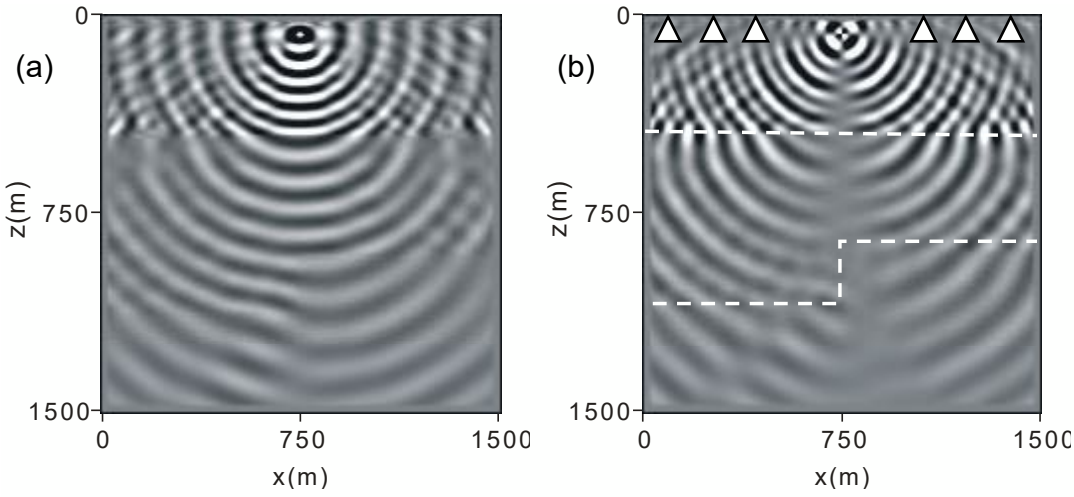

Fig. 5. Real part of 16 Hz monochromatic V_x wavefield (a) and V_z wavefield (b). The horizontal layer and vertical-step layer are delineated with white dashed line on the right panel, which can be easily recognized on the left panel.

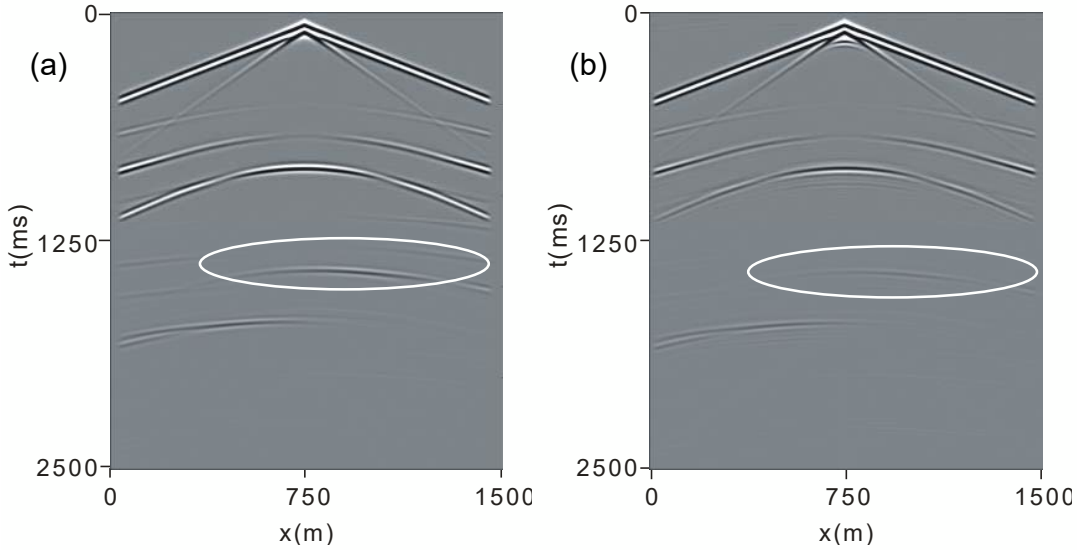

Fig. 6. Synthetic seismograms of horizontal component for vertical-step model from different FD schemes. (a) Staggered grid TDFD (Δt^2, Δx^{20}), (b) staggered grid 4th-order FDFD.

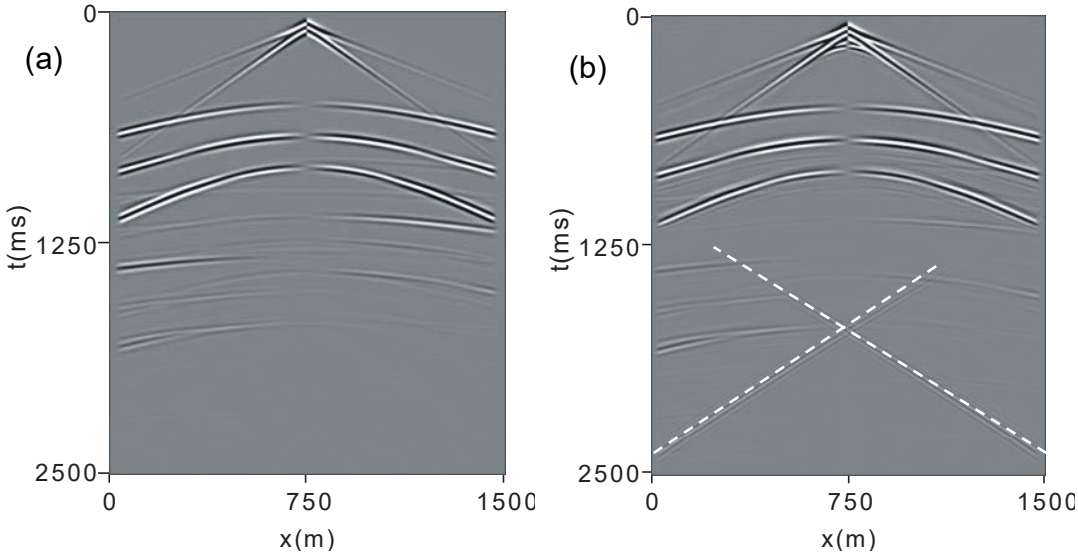

Fig. 7. Synthetic seismograms of vertical component for vertical-step t^2, Δx^{20}), (b) staggered grid 4th-order FDFD.

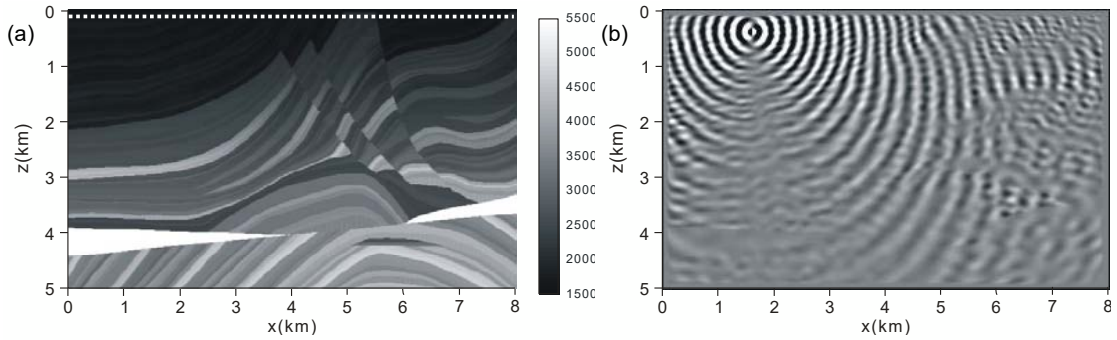

Fig. 8. (a) The *P*-wave velocity distribution of the Marmousi model, (b) The simulated wavefield (real-part) of horizontal velocity component at 8 Hz with $\Delta x = \Delta z = 25$ m by fourth-order FD scheme.

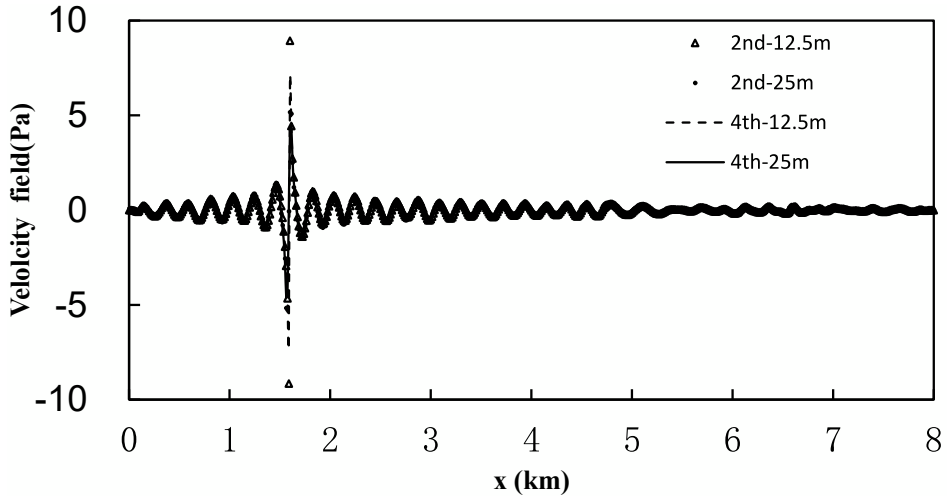

Fig. 9. Comparison of different wavefields by second-order scheme and fourth-order scheme between two grids at 8 Hz.

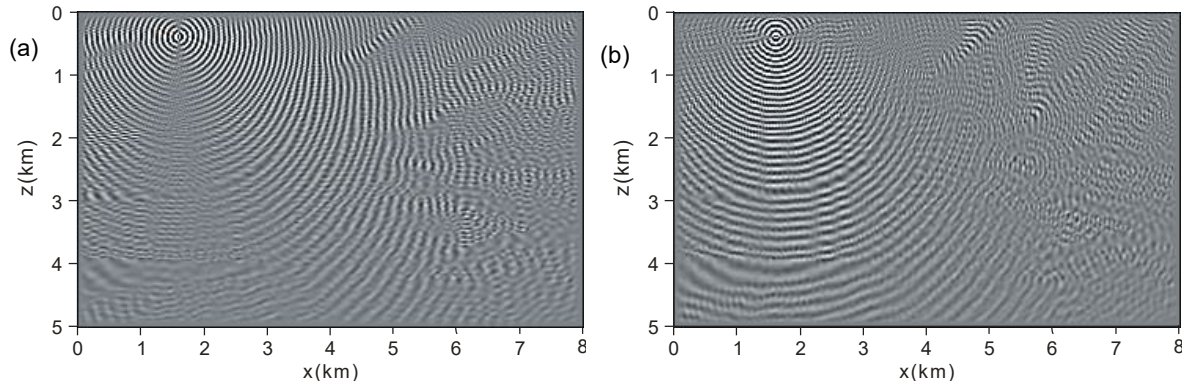

Fig. 10. The simulated wavefield (real-part) at 20 Hz with $\Delta x = \Delta z = 25$ m by fourth-order FD scheme. (a) horizontal component, (b) vertical component.

size of geological model is 8 km × 5 km. The explosive source is excited at x = 1600 m and z = 375 m. Fig. 8b indicates the horizontal velocity component (real part) of 8 Hz monochromatic wavefield.

We pick a line of wavefield from the results of different FD schemes by each grid, while the line is displayed in Fig. 8a. The comparison between them is shown in Fig. 9, which turns out to a perfectly consistence except in the position of source. Regarding the complexity of the model and the dispersion condition between two schemes, under the circumstances of $\Delta x = \Delta z = 25$ m, the second-order scheme could be used to simulate the wavefield when the frequency is as high as 12 Hz, and the results of higher frequency will be dispersed seriously, while the fourth-order scheme keeps its stability at even 20 Hz, the simulated results still manifest the physical significance from the geological model.

4.3 Coupled problem with solid-fluid interface

Seismic simulation for solid-fluid interface problem is a traditional problem in sonic well logging. Here, we construct a simple model by extending the model scale into seismic range, as is shown in Figs. 11a∼b. The model consists of solid matrix with P-wave velocity and S-wave velocity of 3,000 m/s and 1,800 m/s, respectively, and *S*-wave velocity of the water inclusion is zero; the density of solid matrix and water inclusion are 2,000 kg/m^3 and 1,000 kg/m^3 respectively. Fig. 11b reveals a model contains larger fluid area which represents another situation, that is, both source and receiver are placed in the fluid area. We put an impulse source in the position of x = 800 m and z = 400 m, and the wavefield is observed at a receiver downward vertically. Fig. 12a shows the simulation result by conventional FD scheme. It is obvious that at the low frequency wavefield of 5 Hz is distorted severely, and the same effect occurred in the case of borehole measurement as is shown in Fig. 12b, where the simulated wavefield becomes ambiguous when the water inclusion grows.

The modeling results excited at 5 Hz and 50 Hz are presented in Figs. 13a∼b. It is clearly that the staggered grid scheme proposed in this study is capable of dealing with fluid-solid interfacial-coupling problem. Moreover, in order to validate the effectiveness of the staggered grid FDFD in medium with coupled fluid-solid boundary, the model shown in Fig. 11b is used and both the source and receiver are located in borehole fluid surrounded with solid matrix, and the simulation results of horizontal velocity and vertical velocity

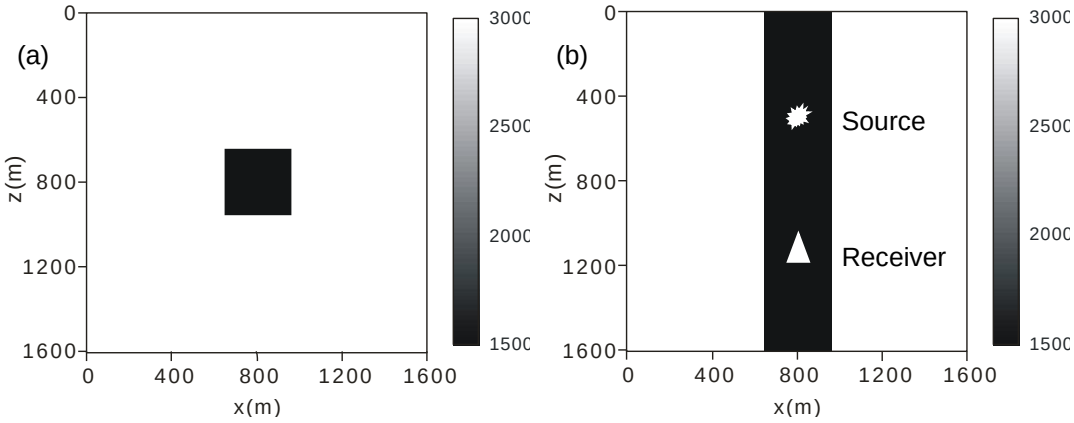

Fig. 11. (a) The P-wave velocity distribution of the disturbance model contains block of fluid with spatial sampling interval equals 8 m. (b) The P-wave velocity distribution of the model contains large fluid area.

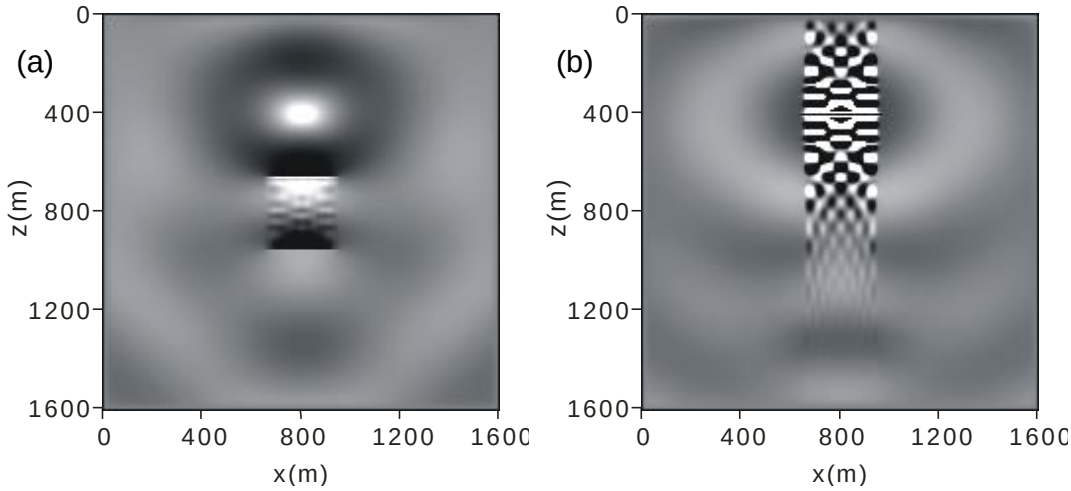

Fig. 12. (a) 5 Hz (real-part) monochromatic (v_x) of model in Fig. 11a calculated by using conventional grid. (a) 5 Hz (real-part) monochromatic (v_x) of model in Fig. 11b calculated by using conventional grid.

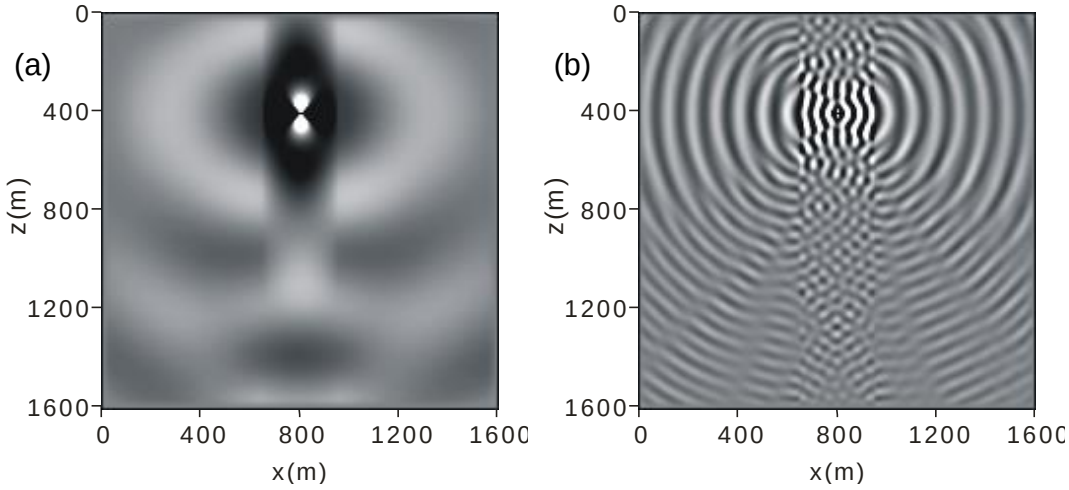

Fig. 13. (a) 5 Hz (real-part) monochromatic (v_x) of model in Fig. 11b calculated by using staggered grid. (b) 50 Hz (real-part) monochromatic (v_x) of model in Fig. 11b calculated by using staggered grid.

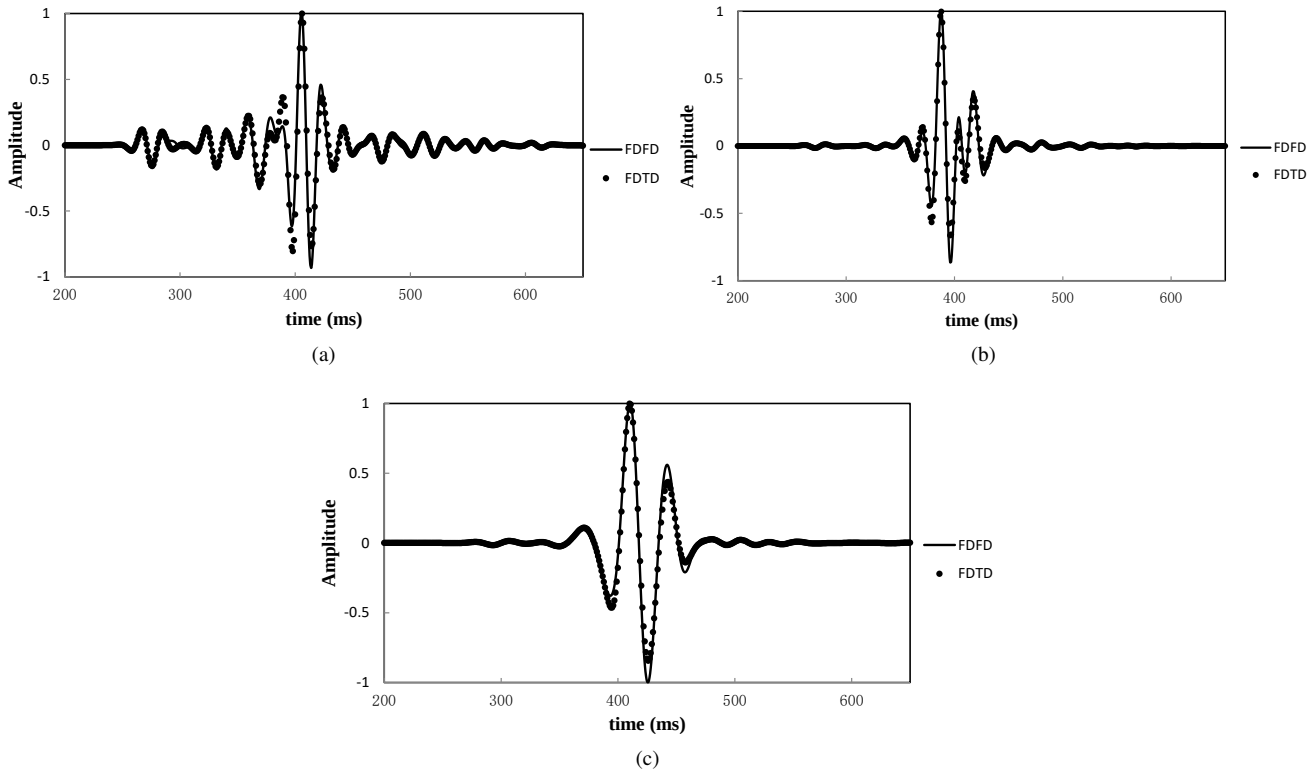

Fig. 14. Normalized amplitude of horizontal velocity (a) and vertical velocity (b) when central frequency is 30 Hz, and vertical velocity (c) when central frequency is 20 Hz from staggered grid FDFD and TDFD solutions.

are shown in Figs. 14a and 14b together with that from the numerical method of TDFD. It is shown that the waveforms from TDFD (Ma and Shen, 2013) and FDFD are matched fairly well on the v_z part for both higher frequency and lower frequency. As a matter of fact, we pose a compressional source in the fluid and the receiver downward, then the received signal is mainly vertical component, the magnitude of horizontal component is lower than 10% of the vertical component.

5. Conclusion

A fourth-order staggered grid finite-difference scheme is developed for elastic wave forward modeling in the frequency-domain. An effective PML absorbing boundary condition is adopted to suppress the artificial reflection. By implementing PML boundary condition and optimizing the FD coefficients, we observe that there is a negligible reflection at the interface between the interior domain and the PML domain. The theoretical dispersion error curve matches well with the numerical one. Moreover, examples contains pure fluid or coupled solid-fluid interfaces demonstrate merits of fourth-order staggered grid finite difference method as follows:

1) By optimizing of the mass weighting coefficients and FD coefficients with Gauss-Newton method, the proposed fourth-order optimal FD scheme accompanied with mass weighted-averaging approach can obtain dispersion curves that are independent of the Poisson's ratio and also acquire high accuracy result in modeling elastic wave propagation.
2) For the homogeneous medium, the simulation error of the shear wave group velocity is within 2%, and only 3 grid points are required per shear wavelength with the same computational efficiency as that of 25-point weighted-averaging FD scheme
3) The staggered grid FD scheme suggested in this study holds the flexibility of modeling in complex medium contains fluid, and when it comes to fluid environment, the elastic system of staggered grid FD scheme will automatically degrade to acoustic one.

The method described above can effectively improve the accuracy of simulation of elastic wave propagation, and also show a satisfactory adaptability for different modeling environment. It could be effectively applied to seismic exploration and acoustic logging, so as to provide services for fine reservoir exploration in oil fields.

Acknowledgments

This research is funded by the National Key R&D Program of China (No. 2018YFC0310002).

References

Arntsen, B., Nebel, A., Amundsen, L. Visco-acoustic finite difference modeling in the frequency domain. J. Seism.

Explor. 1998, 7(1): 45-64.

Bérenger, J.P. A perfectly matched layer for the absorption of electromagnetic waves. J. Comput. Phys. 1994, 114(2): 185-200.

Chillara, V.K., Ren, B., Lissenden, C.J. Guided wave mode selection for inhomogeneous elastic waveguides using frequency domain finite element approach. Ultrasonics 2016, 67: 199-211.

Dablain, M.A. The application of higher order differencing to the scalar wave equation. Geophysics 1986, 51(1): 54-66.

Erlangga, Y., Oosterlee, C., Vuik, C. A novel multigrid based preconditioner for heterogeneous Helmholtz problem. SIAM J. Sci. Comput. 2006, 27(4): 1471-1492.

Gelis, C., Virieux, J., Grandiean, G. Two-dimensional elastic full waveform inversion using Born and Rytov formulations in the frequency domain. Geophys. J. Int. 2007, 168(2): 605-633.

Hustedt, B., Operto, S., Virieux, J. Mixed-grid and staggered-grid finite-difference methods for frequency-domain acoustic wave modelling. Geophys. J. Int. 2004, 157(3): 1269-1296.

Jo, C.H., Shin, C.S., Suh, J.H. An optimal 9 point finite difference frequency-space 2-D wave extrapolator. Geophysics 1996, 61(2): 529-537.

Levander, A.R. Fourth-order finite-difference P-SV seismograms. Geophysics 1988, 53(11): 1425-1436.

Lines, L.R., Treitel, S. Tutorial: A review of least-squares inversion and its application to geophysical problems. Geophys. Prospect. 1984, 32(2): 159-186.

Luo, Y., Schuster, G. Parsimonious staggered grid finite differencing of the wave equation. Geophys. Res. Lett. 1990, 17(2), 155-158.

Ma, C., Shen, J.S. 2D elastic finite-difference modeling of seismic response in fractured anisotropic media. Presented at the 75th EAGE conference & Exhibition incorporating SPE EUROPEC 2013, June, 2013.

Madariaga, R. Dynamics of an expanding circular fault. B. Seismol. Soc. Am. 1976, 66(3): 639-666.

Matuszyk, P.J., Demkowicz, L.F., Torres-Verdin, C. Solution of coupled acoustic-elastic wave propagation problems with anelastic attenuation using automatic hp-adaptivity. Comput. Methods Appl. Mech. Eng. 2012, 213-216: 299-313.

Min, D.J., Shin, C., Kwon, B.D., et al. Improved frequency-domain elastic wave modeling using weighted-averaging difference operators. Geophysics 2000, 65(3): 884-895.

Operto, S., Virieux, J.P., Amestoy, J.L., et al. 3D finite-difference frequency-domain modeling of visco-acoustic wave propagation using a massively parallel direct solver: a feasibility study. Geophysics 2007, 72(5): 195-211.

Pan, G., Abubakar, A., Habashy, T.M. An effective perfectly matched layer design for acoustic fourth-order frequency-domain finite-difference scheme. Geophys. J. Int. 2012, 188(1): 211-222.

Plessix, R.E. A review of the adjoint-state method for computing the gradient of a functional with geophysical applications. Geophys. J. Int. 2006, 167(2): 495-503.

Plessix, R.E. Three-dimensional frequency-domain full-waveform inversion with an iterative solver. Geophysics 2009, 74(6): 149-157.

Pratt, R.G. Frequency-domain elastic wave modeling by finite differences: A tool for crosshole seismic imaging (Short Note). Geophysics 1990a, 55(5): 626-632.

Pratt, R.G. Inverse theory applied to multi-source cross-hole tomography, part 2: Elastic wave-equation method. Geophys. Prospect. 1990b, 38(3): 311-329.

Saenger, E.H., Gold, N., Shapiro, A. Modeling the propagation of elastic waves using a modified finite-difference grid. Wave Motion 2000, 31(1): 77-92.

Shin, C., Sohn, H. A frequency-space 2-D scalar wave extrapolator using extended 25-point finite-difference operator. Geophysics 1998, 63(1): 289-296.

Štekl, I., Pratt, R.G. Accurate viscoelastic modeling by frequency-domain finite differences using rotated operators. Geophysics 1998, 63(5): 1779-1794.

Takekawa, J., Mikada, H. A mesh-free finite-difference method for elastic wave propagation in the frequency-domain. Comput. Geosci. 2018, 118: 65-78.

Virieux, J. SH wave propagation in heterogeneous media, velocity stress finite difference method. Geophysics 1984, 49(11): 1933-1942.

Virieux, J. P-SV wave propagation in heterogeneous media, velocity stress finite difference method. Geophysics 1986, 51(4): 889-901.

Wang, Y., Liang, W. Optimized finite difference methods for seismic acoustic wave modeling, in Computational and Experimental Studies of Acoustic Waves, edited by M. Reyhanoglu, IntechOpen, London, pp. 3-26, 2018.

Appendix: Expressions of the staggered grid finite-difference scheme

From equation system (9), the specific expressions of A_i and B_i (i = 1, … , 8) is as follows:

$$A_1=\frac{-c_{11}(i+1,k)}{S_x(i+\frac{1}{2})S_x(i+1)\rho(i+\frac{1}{2},k)\Delta x^2},\quad A_2=\frac{-c_{13}(i+1,k)}{S_x(i+\frac{1}{2})S_z(k)\rho(i+\frac{1}{2},k)\Delta x\Delta z}$$

$$A_3=\frac{-c_{11}(i,k)}{S_x(i+\frac{1}{2})S_x(i)\rho(i+\frac{1}{2},k)\Delta x^2},\quad A_4=\frac{-c_{13}(i,k)}{S_x(i+\frac{1}{2})S_z(k)\rho(i+\frac{1}{2},k)\Delta x\Delta z}$$

$$A_5=\frac{-c_{55}(i+\frac{1}{2},k+\frac{1}{2})}{S_x(i+\frac{1}{2})S_z(k)\rho(i+\frac{1}{2},k)\Delta x\Delta z},\quad A_6=\frac{-c_{55}(i+\frac{1}{2},k+\frac{1}{2})}{S_z(k)S_z(k+\frac{1}{2})\rho(i+\frac{1}{2},k)\Delta z^2}$$

$$A_7=\frac{-c_{55}(i+\frac{1}{2},k-\frac{1}{2})}{S_x(i+\frac{1}{2})S_z(k)\rho(i+\frac{1}{2},k)\Delta x\Delta z},\quad A_8=\frac{-c_{55}(i+\frac{1}{2},k-\frac{1}{2})}{S_z(k-\frac{1}{2})S_z(k)\rho(i+\frac{1}{2},k)\Delta z^2}$$

$$B_1=\frac{-c_{55}(i+\frac{1}{2},k+\frac{1}{2})}{S_x(i)S_x(i+\frac{1}{2})\rho(i,k+\frac{1}{2})\Delta x^2},\quad B_2=\frac{-c_{55}(i+\frac{1}{2},k+\frac{1}{2})}{S_x(i)S_z(k+\frac{1}{2})\rho(i,k+\frac{1}{2})\Delta x\Delta z}$$

$$B_3=\frac{-c_{55}(i-\frac{1}{2},k+\frac{1}{2})}{S_x(i-\frac{1}{2})S_x(i)\rho(i,k+\frac{1}{2})\Delta x^2},\quad B_4=\frac{-c_{55}(i-\frac{1}{2},k+\frac{1}{2})}{S_x(i)S_z(k+\frac{1}{2})\rho(i,k+\frac{1}{2})\Delta x\Delta z}$$

$$B_5=\frac{-c_{13}(i,k+1)}{S_x(i)S_z(k+\frac{1}{2})\rho(i,k+\frac{1}{2})\Delta x\Delta z},\quad B_6=\frac{-c_{11}(i,k+1)}{S_z(k+\frac{1}{2})S_z(k+1)\rho(i,k+\frac{1}{2})\Delta z^2}$$

$$B_7=\frac{-c_{13}(i,k)}{S_x(i)S_z(k+\frac{1}{2})\rho(i,k+\frac{1}{2})\Delta x\Delta z},\quad B_8=\frac{-c_{11}(i,k)}{S_z(k)S_z(k+\frac{1}{2})\rho(i,k+\frac{1}{2})\Delta z^2}$$

And in the case of fourth-order scheme, the expressions of coefficients $\tilde{A}_1\sim\tilde{A}_{29}$ and $\tilde{B}_1\sim\tilde{B}_{29}$ are combinations of difference coefficient and coefficients A_i and B_i (i = 1, … , 16) for fourth-order scheme.

$$\tilde{A}_1=-a_2^2A_7,\quad \tilde{A}_2=-a_1a_2(A_3+A_7),\quad \tilde{A}_3=(a_1a_2A_1-a_1^2A_3+a_1a_2A_7)$$

$$\tilde{A}_4=-a_2^2A_{16},\quad \tilde{A}_5=-a_1a_2(A_{12}+A_{16}),\quad \tilde{A}_6=a_1a_2A_{10}-a_1^2A_{12}+a_1a_2A_{16}$$

$$\tilde{A}_7=a_1^2(A_1+A_3+A_{10}+A_{12})+a_2^2(A_5+A_7+A_{14}+A_{16}),\quad \tilde{A}_8=-(a_1^2A_{10}-a_1a_2A_{12}-a_1a_2A_{14})$$

$$\tilde{A}_9=-a_1a_2(A_{10}+A_{14}),\quad \tilde{A}_{10}=-a_2^2A_{14},\quad \tilde{A}_{11}=-(a_1^2A_1-a_1a_2A_3-a_1a_2A_5)$$

$$\tilde{A}_{12}=-a_1a_2(A_1+A_5),\quad \tilde{A}_{13}=-a_2^2A_5,\quad \tilde{A}_{14}=-a_2^2(A_8+A_{15})$$

$$\tilde{A}_{15}=-a_1a_2(A_8+A_{11}),\quad \tilde{A}_{16}=a_1a_2(A_8+A_9),\quad \tilde{A}_{17}=a_2^2(A_8+A_{13})$$

$$\tilde{A}_{18}=-a_1a_2(A_4+A_{15}),\quad \tilde{A}_{19}=-a_1^2(A_4+A_{11}),\quad \tilde{A}_{20}=a_1^2(A_4+A_9)$$

$$\tilde{A}_{21}=a_1a_2(A_4+A_{13}),\quad \tilde{A}_{22}=a_1a_2(A_2+A_{15}),\quad \tilde{A}_{23}=a_1^2(A_2+A_{11})$$

$$\tilde{A}_{24}=-a_1^2(A_2+A_9),\quad \tilde{A}_{25}=-a_1a_2(A_2+A_{13}),\quad \tilde{A}_{26}=a_2^2(A_6+A_{15})$$

$$\tilde{A}_{27}=a_1a_2(A_6+A_{11}),\quad \tilde{A}_{28}=-a_1a_2(A_6+A_9),\quad \tilde{A}_{29}=-a_2^2(A_6+A_{13})$$

$$\tilde{B}_1=-a_2^2(B_8+B_{15}),\quad \tilde{B}_2=-a_1a_2(B_8+B_{11}),\quad \tilde{B}_3=a_1a_2(B_8+B_9)$$

$$\tilde{B}_4=a_2^2(B_8+B_{13}),\quad \tilde{B}_5=-a_1a_2(B_4+B_{15}),\quad \tilde{B}_6=-a_1^2(B_4+B_{11})$$

$$\tilde{B}_7=a_1^2(B_4+B_9),\quad \tilde{B}_8=a_1a_2(B_4+B_{13}),\quad \tilde{B}_9=a_1a_2(B_2+B_{15})$$

$$\tilde{B}_{10}=a_1^2(B_2+B_{11}),\quad \tilde{B}_{11}=-a_1^2(B_2+B_9),\quad \tilde{B}_{12}=-a_1a_2(B_2+B_{13})$$

$$\tilde{B}_{13}=a_2^2(B_6+B_{15}),\quad \tilde{B}_{14}=a_1a_2(B_6+B_{11}),\quad \tilde{B}_{15}=-a_1a_2(B_6+B_9)$$

$$\tilde{B}_{16}=-a_2^2(B_6+B_{13}),\quad \tilde{B}_{18}=-a_1a_2(B_3+B_7),\quad \tilde{B}_{17}=-a_2^2B_7$$

$$\tilde{B}_{19}=(a_1a_2B_1-a_1^2B_3+a_1a_2B_7),\quad \tilde{B}_{20}=-a_2^2B_{16},\tilde{B}_{21}=-a_1a_2(B_{12}+B_{16})$$

$$\tilde{B}_{22} = (a_1a_2B_{10} - a_1^2B_{12} + a_1a_2B_{16}), \quad \tilde{B}_{23} = \left[a_1^2(B_1 + B_3 + B_{10} + B_{12}) + a_2^2(B_5 + B_7 + B_{14} + B_{16})\right]$$

$$\tilde{B}_{24} = -(a_1^2B_{10} - a_1a_2B_{12} - a_1a_2B_{14}), \quad \tilde{B}_{25} = -a_1a_2(B_{10} + B_{14}),$$

$$\tilde{B}_{26} = -a_2^2B_{14}, \quad \tilde{B}_{27} = -(a_1^2B_1 - a_1a_2B_3 - a_1a_2B_5), \quad \tilde{B}_{28} = -a_1a_2(B_1 + B_5), \quad \tilde{B}_{29} = -a_2^2B_5$$

where the specific expressions of A_i and B_i (i = 1, … , 16) is as follows:

$$A_1 = c_{11}(i+1,k)/[\omega^2\rho_x S_x(i+\frac{1}{2})S_x(i+1)\Delta x^2], \quad A_2 = c_{13}(i+1,k)/[\omega^2\rho_x S_x(i+\frac{1}{2})S_z(k)\Delta x\Delta z]$$

$$A_3 = c_{11}(i,k)/[\omega^2\rho_x S_x(i+\frac{1}{2})S_x(i)\Delta x^2], \quad A_4 = c_{13}(i,k)/[\omega^2\rho_x S_x(i+\frac{1}{2})S_z(k)\Delta x\Delta z]$$

$$A_5 = c_{11}(i+2,k)/[\omega^2\rho_x S_x(i+\frac{1}{2})S_x(i+2)\Delta x^2], \quad A_6 = c_{13}(i+2,k)/[\omega^2\rho_x S_x(i+\frac{1}{2})S_z(k)\Delta x\Delta z]$$

$$A_7 = c_{11}(i-1,k)/[\omega^2\rho_x S_x(i+\frac{1}{2})S_x(i-1)\Delta x^2], \quad A_8 = c_{13}(i-1,k)/[\omega^2\rho_x S_x(i+\frac{1}{2})S_z(k)\Delta x\Delta z]$$

$$A_9 = c_{55}(i+\frac{1}{2},k+\frac{1}{2})/[\omega^2\rho_x S_x(i+\frac{1}{2})S_z(k)\Delta x\Delta z], \quad A_{10} = c_{55}(i+\frac{1}{2},k+\frac{1}{2})/[\omega^2\rho_x S_z(k)S_z(k+\frac{1}{2})\Delta z^2]$$

$$A_{11} = c_{55}(i+\frac{1}{2},k-\frac{1}{2})/[\omega^2\rho_x S_x(i+\frac{1}{2})S_z(k)\Delta x\Delta z], \quad A_{12} = c_{55}(i+\frac{1}{2},k-\frac{1}{2})/[\omega^2\rho_x S_z(k)S_z(k-\frac{1}{2})\Delta z^2]$$

$$A_{13} = c_{55}(i+\frac{1}{2},k+\frac{3}{2})/[\omega^2\rho_x S_x(i+\frac{1}{2})S_z(k)\Delta x\Delta z], \quad A_{14} = c_{55}(i+\frac{1}{2},k+\frac{3}{2})/[\omega^2\rho_x S_z(k)S_z(k+\frac{3}{2})\Delta z^2]$$

$$A_{15} = c_{55}(i+\frac{1}{2},k-\frac{3}{2})/[\omega^2\rho_x S_x(i+\frac{1}{2})S_z(k)\Delta x\Delta z], \quad A_{16} = c_{55}(i+\frac{1}{2},k-\frac{3}{2})/[\omega^2\rho_x S_z(k)S_z(k-\frac{3}{2})\Delta z^2]$$

$$B_1 = c_{55}(i+\frac{1}{2},k+\frac{1}{2})/[\omega^2\rho_z S_x(i)S_x(i+\frac{1}{2})\Delta x^2], \quad B_2 = c_{55}(i+\frac{1}{2},k+\frac{1}{2})/[\omega^2\rho_z S_x(i)S_z(k+\frac{1}{2})\Delta x\Delta z]$$

$$B_3 = c_{55}(i-\frac{1}{2},k+\frac{1}{2})/[\omega^2\rho_z S_x(i)S_x(i-\frac{1}{2})\Delta x^2], \quad B_4 = c_{55}(i-\frac{1}{2},k+\frac{1}{2})/[\omega^2\rho_z S_x(i)S_z(k+\frac{1}{2})\Delta x\Delta z]$$

$$B_5 = c_{55}(i+\frac{3}{2},k+\frac{1}{2})/[\omega^2\rho_z S_x(i)S_x(i+\frac{3}{2})\Delta x^2], \quad B_6 = c_{55}(i+\frac{3}{2},k+\frac{1}{2})/[\omega^2\rho_z S_x(i)S_z(k+\frac{1}{2})\Delta x\Delta z]$$

$$B_7 = c_{55}(i-\frac{3}{2},k+\frac{1}{2})/[\omega^2\rho_z S_x(i)S_x(i-\frac{3}{2})\Delta x^2], \quad B_8 = c_{55}(i-\frac{3}{2},k+\frac{1}{2})/[\omega^2\rho_z S_x(i)S_z(k+\frac{1}{2})\Delta x\Delta z]$$

$$B_9 = c_{13}(i,k+1)/[\omega^2\rho_z S_x(i)S_z(k+\frac{1}{2})\Delta x\Delta z], \quad B_{10} = c_{11}(i,k+1)/[\omega^2\rho_z S_z(k+\frac{1}{2})S_z(k+1)\Delta z^2]$$

$$B_{11} = c_{13}(i,k)/[\omega^2\rho_z S_x(i)S_z(k+\frac{1}{2})\Delta x\Delta z], \quad B_{12} = c_{11}(i,k)/[\omega^2\rho_z S_z(k+\frac{1}{2})S_z(k)\Delta z^2]$$

$$B_{13} = c_{13}(i,k+2)/[\omega^2\rho_z S_x(i+\frac{1}{2})S_z(k)\Delta x\Delta z], \quad B_{14} = c_{11}(i,k+2)/[\omega^2\rho_z S_z(k+\frac{1}{2})S_z(k+2)\Delta z^2]$$

$$B_{15} = c_{13}(i,k-1)/[\omega^2\rho_z S_x(i+\frac{1}{2})S_z(k)\Delta x\Delta z], \quad B_{16} = c_{11}(i,k-1)/[\omega^2\rho_z S_z(k+\frac{1}{2})S_z(k-1)\Delta z^2]$$

where, $\rho_x = \rho(i+\frac{1}{2},k)$, $\rho_z = \rho(i,k+\frac{1}{2})$, $S_n = i\omega + d_n$.